



ELSEVIER

Journal of Photochemistry and Photobiology A: Chemistry 142 (2001) 197–207

Journal of
Photochemistry
and
Photobiology
A: Chemistry

www.elsevier.com/locate/jphotochem

Photothermal conversion dynamics in femtosecond and picosecond discrete laser etching of Cu-phthalocyanine amorphous film analysed by ultrafast UV–VIS absorption spectroscopy

Yoichiroh Hosokawa, Masaki Yashiro, Tsuyoshi Asahi¹, Hiroshi Masuhara**Department of Applied Physics, Faculty of Engineering, Osaka University, Yamadaoka 2-1, Suita, Osaka 565-0871, Japan*

Abstract

Novel etching of Cu-phthalocyanine (CuPc) amorphous film which is characteristic of ultrashort laser irradiation was successfully confirmed by tuning Ti:Sapphire laser (780 nm) to 150 fs, 250 ps, or 100 ns, and the primary processes were investigated by fs pump-fs probe and ps pump-fs probe spectroscopic measurements. In the fs and ps laser ablation, we have found discrete laser etching in that the etch depth becomes constant and is independent of laser fluence above the ablation threshold, although gradual (normal) etching, in which the etch depth increase continuously with the fluence above ablation threshold, was observed in the ns laser ablation. The transient absorption spectral measurements reveal the nonlinear photothermal conversion processes, corresponding to exciton–exciton annihilation and cyclic multiphotonic absorption. Their time evolutions during and after the excitation pulse duration were considered and elucidated to depend strongly on the excitation pulse width. On the basis of these results, we discuss an ablation mechanism for the ps and fs ablation that the temperature elevation bringing about transient high pressure is responsible for discrete etching. © 2001 Published by Elsevier Science B.V.

Keywords: Discrete etching; Femtosecond laser ablation; Photothermal conversion; Cu-phthalocyanine; Transient absorption spectroscopy

1. Introduction

Since the flash photolysis method was first proposed by Norrish and Porter in 1949 [1], time-resolved UV–VIS absorption spectroscopy has contributed greatly to studies of chemical, physical, and biological processes. Excited states and transient chemical species have been identified, their relaxation/reaction rates have been directly determined, and in turn, this has allowed molecular mechanisms to be elucidated in detail. The temporal resolution has been improved from ms to μ s, from ns to ps, and now from sub-ps to real fs by introducing various kinds of pulsed laser excitation and monitoring light sources [2,3]. Absorption spectroscopic measurements have typically been performed on optically clear samples such as transparent films, gaseous, and solution systems; in other words, transmittance-mode optical alignment has usually been applied. The spectroscopic measurement, however, is sometimes difficult, since some materials have large extinction coefficients and photophysical/photochemical processes are induced only in the surface

layers and living systems like biocells are opaque or translucent rather than optically transparent. Thus, simple application of conventional transmittance-mode spectroscopy is prevented, so that the interesting photoprocesses of such materials and living systems remain largely unknown.

Various methods have been proposed for elucidating solid surface dynamics and applied by many researchers; for example, Auston and Shank developed ps ellipsometry [4]. In general, surface processes can be probed by regular reflection spectroscopy, and transient reflectance difference spectral experiments have been reported. Also, various analysis methods were designed and applied for measurements of complex refractive index spectra [5–10]. We have developed ps and fs measurement systems for obtaining time-resolved extinction and refractive index change spectra and applied them to phthalocyanine solids [11–14].

For optically scattering materials, Wilkinson and coworkers proposed a ns diffuse reflectance spectroscopic method and analysed its optical requirements in 1981 [15,16], which, in principle, are based on Kubelka–Munk theory [17]. A few years later, we were able to improve the time-resolution to ps [18–20], and as a result, the photoprocesses of organic microcrystals, semiconductor photocatalysis, insoluble polymer powders, molecules adsorbed on metal oxides and zeolites, and so on, became as accessible to study as

* Corresponding author. Tel.: +81-6-6879-7837; fax: +81-6-6876-8580.

E-mail addresses: asahi@ap.eng.osaka-u.ac.jp (T. Asahi),

masuhara@ap.eng.osaka-u.ac.jp (H. Masuhara).

¹ Co-corresponding author.

transparent solutions. Recently, fs diffuse reflectance spectroscopy has been developed through the introduction of fs laser pulses and their white continuum as pump and probe pulses, respectively [21]. Systematic data on ultrafast processes in optically scattering solids and colloidal solutions can be acquired, but their temporal analysis is not so simple as fs pulses become broad during propagation in scattering materials. Thus, it was necessary and indispensable to analyse the propagation of fs pulses and to evaluate their temporal resolution, as well as to compare the simulated curves with experimental data. Now fs pump-fs probe diffuse reflectance spectroscopy is indispensable [21,22] and used mainly for revealing ultrafast charge separation and recombination, and chemical primary processes in photocatalysts [23–25].

The pump-probe time-resolved measurements are not limited to spectroscopy for photophysics and photochemistry, but can be applied to various dynamics studies on materials. For example, shadowgraphy, interferometry, scattering imaging, and so on based on pump-probe methods have shown high potential in elucidating laser ablation phenomena. Time-resolved shadowgraphy [26,27] was performed to observe side-view pictures about laser excited material surface at different delay times after excitation. How shockwave and fragmentation develop in space is clearly demonstrated, and the propagation and ejection rates were directly determined. Ns interferometry, where excimer laser and 2nd harmonics of ns Nd³⁺:YAG laser are used as pump and probe pulses, respectively, was developed and applied mainly to polymer ablation by us [28–32]. By analysing time-dependent fringe shifts of the interference patterns, it was first clarified that some polymer films undergo expansion even below ablation threshold and accompanying surface displacement behaviour was obtained. The dynamics was elucidated with resolutions of ~10 nm and 10 ns. PMMA and polystyrene films start to expand during the excitation pulse width and undergo fragmentation leading to ablation, while the former shows interesting nm–ns oscillatory expansion and contraction dynamics for below ablation threshold. Earlier processes in surface morphology changes are followed by a time-resolved surface light scattering imaging [33–35]. After high intense fs laser irradiation, originally flat surfaces of liquids and organic thin films become rough and scatter the fs probe pulses to the hemisphere. Hence, surface roughness formation in the scale of nm can be estimated by monitoring the time evolution of the scattered light.

Such investigations and experiments by pump-probe methods are now regarded as important and indispensable to reveal the nature of morphological dynamics with both fs–ns and nm resolution. Ultrafast intense excitation of organic materials creates high density excited states, and electronic relaxation involves mutual interactions between excitons, ionisation, local heating, stress formation due to photochemical and photothermal processes, in addition to normal photophysics. Further increase in the excitation

intensity results in laser ablation, etching, fabrication, and melting phenomena. If pump-probe spectroscopy is applied to investigating such morphological changes as described above, how electronic excitation energy evolves to surface morphology dynamics can be clarified. The approach is receiving much interest in the relevant fields and is opening a new way to understand morphological dynamics in terms of electronic and molecular processes.

In the present work, this approach has been performed for understanding the mechanism of laser ablation of Cu-phthalocyanine (CuPc) amorphous films. As a first sample to investigate the photoprimary processes, we selected an amorphous film, because optically anisotropic and mechanically complex properties due to crystal structure are excluded. Also CuPc is a molecule whose photophysical processes are well studied by time-resolved absorption spectroscopy. We have already demonstrated that the etching behaviour of CuPc microcrystalline films is strongly depend on the excitation pulse duration (170 fs, 250 ps, 100 ns) of a 780 nm Ti:Sapphire laser [35]. In the investigation, above the fs and ps ablation thresholds, the etch depth became constant and was almost independent of laser fluence, which we named discrete etching. On the other hand, the depth etched by ns laser excitation increases gradually with the fluence above its ablation threshold. Even when almost same number of photons at the same 780 nm wavelength are absorbed, the etching depends strongly on the pulse width. Thus, it should be very interesting to reveal photoprimary processes in fs–ns time range.

First we report here the pulse duration dependence of laser etching for CuPc amorphous film instead of the microcrystalline film. Then, we report the photoprimary processes depending of the excitation pulse width from results of fs pump-fs probe and ps pump-fs probe spectroscopic measurements. In the case of fs ablation, single-shot absorption spectroscopy probes the transient species and morphologies created by impulsive excitation, which is quite normal and useful as in linear photophysical and photochemical studies. On the other hand, in the case of ps ablation, it is very interesting and possible to reveal dynamics of excited states annihilation, cyclic multiphotonic absorption [36], photothermal heating, etc. during laser excitation with fs probe pulse. On the basis of these results, we will discuss the ablation mechanism and its dependence on the excitation pulse width.

2. Experimental

2.1. Materials

Amorphous films of tetra-(*N*-(2-ethylhexyl)-sulfamoyl)-substituted CuPc (Savinyl Blue GLS, Mitsui Toatsu Chemicals, Inc., hereafter abbreviated to SB) were prepared by a casting technique. An ethanol (HPLC grade, Nacalai Tesque Inc.) solution of SB (3.0×10^{-3} M) was spread on a quartz substrate and dried in air for 1 day. The films are optically

transparent and thicknesses were 300–600 nm, giving an absorption coefficient (α) of $0.7 \mu\text{m}^{-1}$.

2.2. Excitation pulse characteristics

Femtosecond laser pulses from an Ar^+ laser-pumped Ti:Sapphire laser (Coherent, Mira Basic, 780 nm, 76 MHz) were amplified by a Ti:Sapphire chirped-pulse amplification laser system (Continuum, TR70-10, 780 nm). The amplified laser pulse after the compression was used as a fs light source. The typical output has 170 fs fwhm and 3 mJ/pulse energy. The ps laser pulse with 250 ps fwhm is provided when the amplified pulse was not compressed. When the regenerative amplifier is not seeded by the oscillator, a ns laser pulse with 100 ns fwhm is obtained. The spectral and temporal profile of the excitation pulses is shown in Fig. 1. The temporal profile of the fs pulse is given as an auto-correlation trace measured by second harmonic generation. The profile of the chirped ps and ns pulse were directly measured by a streak camera (Hamamatsu, C4334) and by a pin photodiode (Thorlabs, 201/579-7227), respectively. The temporal profile of each laser beam was confirmed to have a Gaussian distribution. Their spatial profiles were also confirmed to have a Gaussian distribution by a CCD camera (Sony, XC-7500). One shot pulse was picked up as an excitation beam from the pulse train with

the frequency of 10 Hz by a mechanical shutter and focused on the film surface through a lens ($f = 30 \text{ cm}$) with a spot size of a few 100 nm. Etching behaviour was observed by an optical microscope (Olympus, BX 50) and the etching profile was measured by a stylus profiler (Sloan, Dektak).

2.3. Femtosecond/picosecond pump-femtosecond probe absorption spectroscopy

The femtosecond absorption spectroscopy system is a conventional one used in our laboratory [37,38]. Excited and transient states created with the fs 780 nm pulse as described above are probed by a fs white light continuum (400–700 nm, 170 fs fwhm), which was generated by focusing the 780 nm pulse into H_2O . The delay time zero was defined as the time when both fs pulses have maximum overlap. For fs spectral measurement, the chirping (dispersion) of the white continuum should be considered for correct and reliable analysis. The temporal dispersion of the white light continuum was estimated by measuring the time correlation profile between the white continuum and the excitation light [37], and transient absorption spectra were corrected by using this time dispersion profile.

The picosecond pump-fs probe absorption spectroscopic system is shown in Fig. 2. Half of the amplified pulse was deflected and used as ps excitation pulse, while the residual pulse was compressed and the obtained fs was used similarly for producing the white light continuum. Mechanical shutters are used for picking up one pair of ps and fs pulses from the 10 Hz repetitions. The origin of the time axis was defined as the time when the ps laser pulse reach a maximum intensity. The fs probe light was detected by a pair of polychromators coupled with multichannel photodiode arrays (Otsuka Electronics, MCPD HH4-0913). A transient absorption spectrum was obtained by averaging 300 shots of the probe light, when the laser fluence of the excitation pulse is below ablation threshold. Each measurement upon laser ablation was done for a virgin surface of SB film by changing the sample position from shot to shot, and the absorption spectra at each delay time were obtained by averaging 10 measurements.

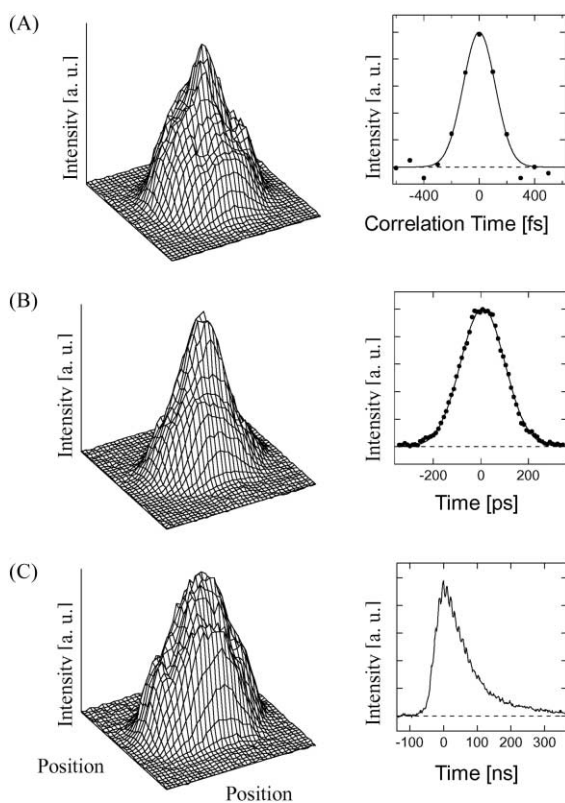


Fig. 1. Spatial and temporal profiles of (A) fs, (B) ps, and (C) ns excitation pulses.

3. Results and discussion

3.1. Discrete and gradual laser etching depending on excitation pulse width

Microphotographs of the SB film after single-shot irradiation of Ti:Sapphire laser with 170 fs, 250 ps, and 100 ns pulse duration are summarised in Fig. 3. On the surface etched by fs laser, there were many cracks with a few $10 \mu\text{m}$ spacing. The etched area increases with the laser fluence above the ablation threshold due to the Gaussian-like spatial profile of the laser beam. Edges of ablated patterns were sharp, which

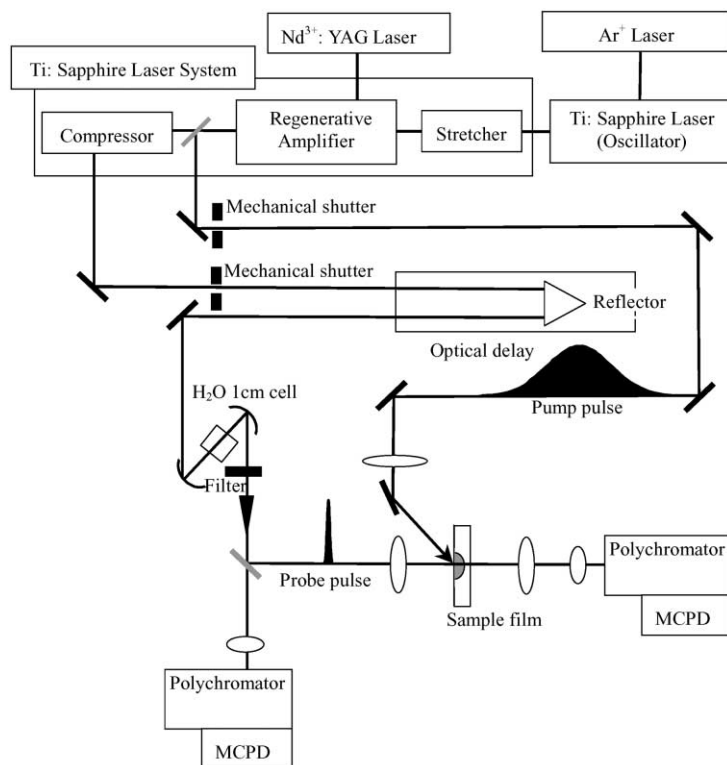


Fig. 2. An experimental set-up of the ps pump-fs probe absorption spectroscopic system.

was confirmed by surface etching profile measurement. Similar etching patterns and profiles were observed in ps laser ablation, while the ablation threshold (80 mJ/cm^2) is higher than the fs one (35 mJ/cm^2). On the other hand, no crack and smooth slope without sharp edges was observed

for ns laser ablation. The latter threshold of 140 mJ/cm^2 is higher than those of fs and ps cases. Many dark spots in the microphotographs before irradiation can be considered to be local humps. In all cases, there was no obvious correlation between the spots and etching behaviours, so that we

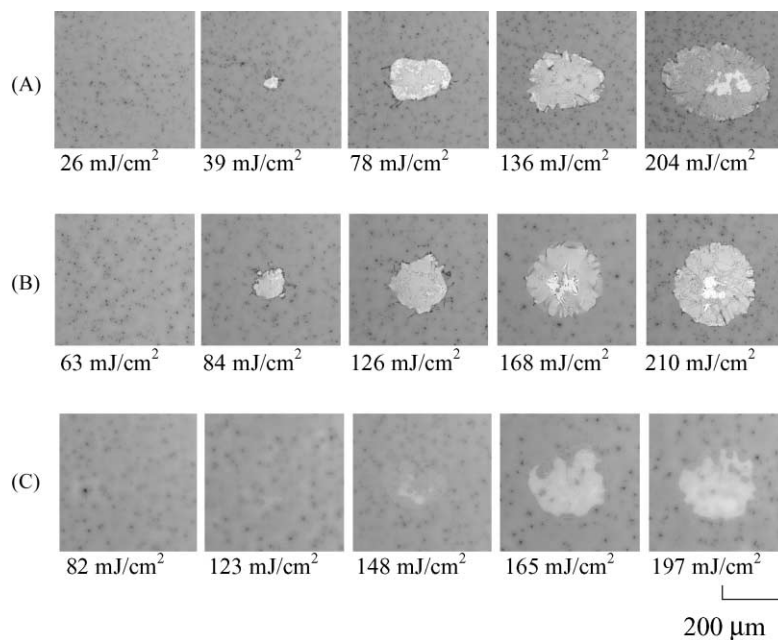


Fig. 3. Optical transmission images of SB film after being exposed to (A) 170 fs, (B) 250 ps, and (C) 100 ns single laser pulses. Laser fluence and dimension are given in the figure.

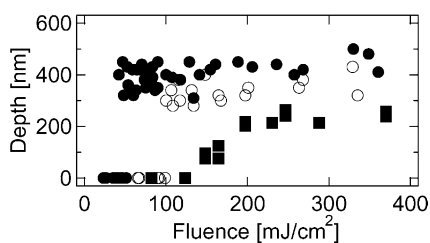


Fig. 4. Plot of etch depth vs. laser fluence for (●) 170 fs, (○) 250 ps, and (■) 100 ns laser pulses.

consider contribution of the dark spots can be negligible in the ablation.

Relations between the etch depth and laser fluence are summarised in Fig. 4. In fs and ps laser ablation, the etch depth becomes constant and is independent of laser fluence above ablation threshold, which we already named discrete etching [34,35]. On the other hand, the etch depth by ns laser ablation increases gradually with laser fluence above the threshold, which is quite general for many materials. Femtosecond etching behaviour has been examined, and plasma generation and incubation effects due to transient species and photoproducts are discussed in relation to ablation mechanism [39–44]. However, for the first time to our knowl-

edge, we have confirmed discrete etching. How the etching is brought about is considered here by examining dynamics by following electronic excitation and relaxation dynamics with ultrafast UV–VIS absorption spectroscopy.

3.2. Temperature difference absorption spectra of the ground state

Ground state absorption spectra of SB film and its solutions are shown in Fig. 5A, where the Q-band with two peaks at 620 and 680 nm appears. For crystalline CuPc, the Q-band shape is clearly observed and considered to be due to Davydov splitting, which comes from π to π overlap intermolecular configuration in the crystal [45]. In contrast, the present SB film takes an amorphous structure, which is confirmed by a broad X-ray diffraction pattern [46]. The most possible explanation of the splitting in SB film is due to local aggregation of SB molecules and the possibility was checked by examining concentration dependence of SB solution. The results of the ground state absorption spectra are summarised in Fig. 5A. One intense peak at 670 nm and a shoulder at 600 nm were obtained in the concentration of 1.5×10^{-6} M, while the relative intensity of the peak at 620 nm increases with increasing concentration. When the concentration was adjusted to 3×10^{-3} M, two peaks at 620

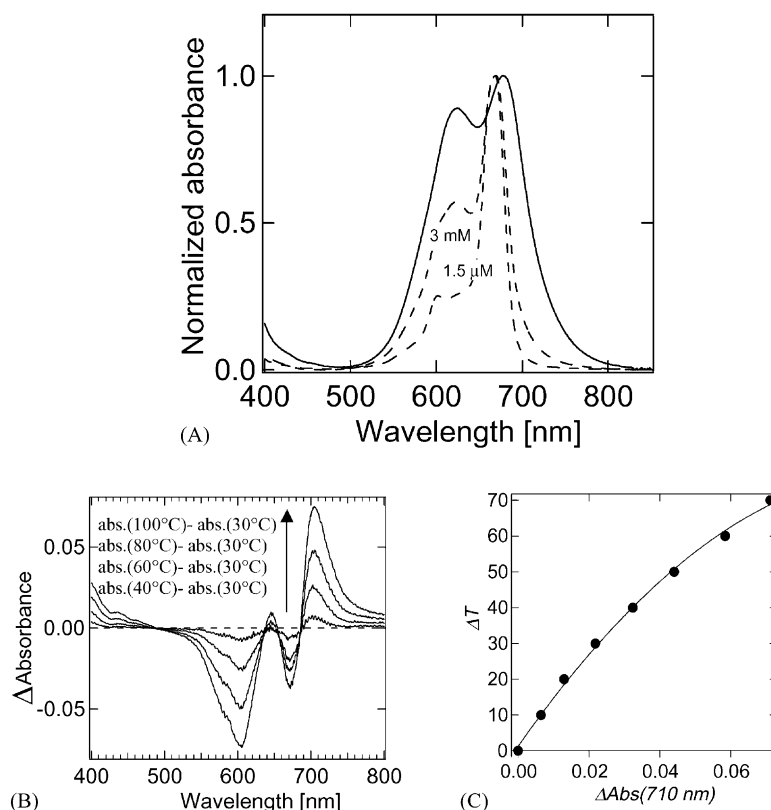


Fig. 5. (A) Ground state absorption spectra of SB film (solid line) and ethanol solution (dashed line) with SB concentration of 3×10^{-3} and 1.5×10^{-6} M. Three spectra are normalised at maximum peak wavelength. (B) Temperature difference spectra of SB film obtained by subtracting the spectrum at room temperature (30°C) from that at 40, 60, 80, and 100°C. (C) Plots of the temperature difference vs. absorbance difference at 710 nm. Solid line is calculated and fitted by a quadratic function (see text).

and 670 nm were clearly observed. The concentration dependence suggests that the band at 620 nm is relatively strong compared to that at 670 nm upon dimer/aggregation. Q-band transitions of SB film can be identified similarly, while the peak shifted from 670 to 680 nm, which will be ascribed to an environmental effect in viewpoint that amorphous film is a kind of high dense neat solution. Note that, at the excitation wavelength of 780 nm, the absorption coefficient of the dimer/aggregate is stronger than that of the monomer, because the shoulder above 700 nm increases with increasing the concentration of the dimer/aggregate.

The ground state spectra of SB film was measured at some temperatures, and their difference spectra were obtained by subtracting the spectrum at room temperatures (30°C) from that at higher temperatures. The difference arises from vibrational excitation of the electronically ground state, which is assigned to a hot band of the latter state. It was experimentally confirmed (Fig. 5B) that the difference increases with temperature elevation, but its spectral shape also depends slightly on the temperature. The absorbance difference at 710 nm, $\Delta\text{Abs}(710\text{ nm})$, was empirically fitted by the following quadratic function of temperature difference, ΔT .

$$\Delta\text{Abs}(710\text{ nm}) = 5.25 \times 10^{-4} \times \Delta T + 7.18 \times 10^{-6} \times \Delta T^2 \quad (1)$$

The experimental data are well reconstructed by the equation as shown in Fig. 5C. By applying the equation to transient absorption spectra, we can estimate temperature change as a function of delay time in laser ablation. In the present work, we discuss transient absorption spectra by taking account the interpretation of the ground state absorption spectra.

3.3. Femtosecond pump-femtosecond probe absorption spectra under laser ablation

Transient absorption spectra at 0.5 ps after excitation were measured at several laser fluences, and typical spectra for fluence below and above ablation threshold (35 mJ/cm²) are shown in Fig. 6A. A broad positive absorption was observed around 520 nm, which can be assigned to the electronically excited states of SB [12,34]. Negative absorption corresponds to that of the ground state, meaning the latter state depletion upon excitation. We have already reported similar transient absorption spectra of CuPc microcrystalline solids [11,14,35], however, a drastic change depending on laser fluence in the negative absorption was found only for SB film. It suggests that the spectral characteristic originates in the amorphous structure. The negative absorption in the visible region at the fluence of 1.5 mJ/cm² is broad and the peak is at 620 nm. The negative intensity increases with fluence, and a new peak appears at 680 nm. The spectral shape at 100 mJ/cm² is similar to the reverse of the ground state absorption.

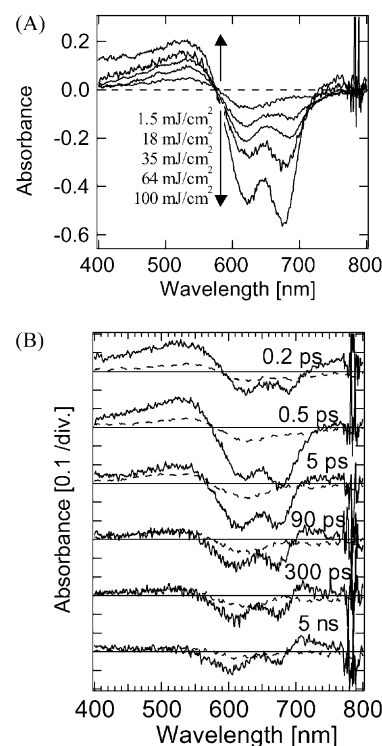


Fig. 6. (A) Fluence dependence of fs pump-fs probe absorption spectra at 0.5 ps. Laser fluences are given in the figure. (B) Femtosecond pump-fs probe absorption spectra at the laser fluence of 64 mJ/cm² (solid line) and 1.5 mJ/cm² (broken line). Delay times are given in the figure.

As the absorption coefficient of the dimer/aggregate is stronger than that of monomer at 780 nm, it is reasonable to consider that the dimer/aggregate can be excited more efficiently. As a result, the ground state absorption at 620 nm will relatively bleach at first. With increasing the fluence, the depletion of the ground state dimer/aggregate will take place and monomer will be excited efficiently, i.e. the bleaching at 680 nm means that the monomer depletion also becomes appreciable. As the absorption coefficient of monomer is very weak at the excitation wavelength, there is a possibility that the following nonlinear processes are involved in addition to the linear absorption. (1) The monomer absorbs photons through simultaneous multiphoton absorption. (2) The excitation energy is transferred to monomer from higher excited states of the dimer/aggregate, which is generated through their exciton–exciton annihilation. These nonlinear absorption processes are realised more efficiently in fs excitation than in the ps case. The time profile of absorption at 520 nm is shown in Fig. 7A. It is clear that the absorption due to the excited states decay faster with increasing laser fluence. The time dependence can be assigned to exciton–exciton annihilation, which is reported by many groups [11–14,47,48]. As the annihilation is appreciable when the ground state dimer/aggregate molecules are depleted and, thus, more of monomer molecules are excited, it will be controlled by strong coupling between

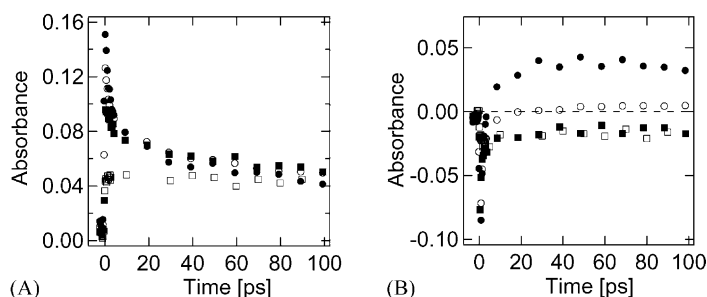


Fig. 7. Temporal profiles of transient absorption at 520 (A) and 710 (B) nm at the laser fluence of 64 mJ/cm² (●), 35 mJ/cm² (○), 18 mJ/cm² (■), and 1.5 mJ/cm² (□) in fs pump-fs probe experiment.

neighbouring excited molecules such as the Dexter-type interaction between dimer/aggregate molecules.

With increase in the delay time, positive and negative peaks at low laser fluence disappear simultaneously and monotonously, and a positive peak appears at 710 nm at late stage as shown in Fig. 6B. The spectrum observed at 5 ns is similar to the temperature difference spectra in Fig. 5B. When the excited states are created densely, an efficient interaction between excited states such as exciton–exciton annihilation will be favoured, giving hot band ground state absorption. Time profiles of absorption at 710 nm are shown in Fig. 7B, where the bleaching of ground states are overlapped. The time profile in the time region up to 5 ps is considered to be due to generation and recovery of the bleaching. The contribution of the hot band recovery overcomes that of the bleaching at late stage 20 ps after excitation at the fluence of 35 and 64 mJ/cm². The time scale to recover the bleaching is similar to the fast decay of the excited states. Therefore, it is concluded that temperature elevation take place practically up to 20 ps at the fluence above the threshold, although the rate depends on the fluence because of exciton–exciton annihilation.

3.4. Picosecond pump-femtosecond probe absorption spectra under laser ablation

The transient spectra of SB film within 250 ps excitation pulse were measured by a fs white light continuum. The transient spectra at the fluence of 9.7 and 112 mJ/cm² are given in Fig. 8. As the ps ablation threshold is 80 mJ/cm², the spectral change at 112 mJ/cm² reflects photophysical processes leading to ablation at a later stage. A positive absorption around 520 nm and a negative absorption with a peak at 620 nm are maximal at 0 ps. After 0 ps, another negative peak was detected at 680 nm and its intensity increased almost up to a few hundred ps. Corresponding to the decay of the 520 nm band, the positive absorption around 710 nm is increased and the negative peak at 620 nm is shifted to at 610 nm. After the positive band around 520 nm has mostly decayed, the positive band around 710 nm and the negative band with peaks at 600 and 680 nm still remained. At weak enough laser fluence, typically 9.7 mJ/cm², the positive

band around 710 nm and negative peaks at 610 and 680 nm were not observed clearly. The spectral shape with positive band around 520 nm and the negative band with peak at 620 nm are observed even in ns time region, although the intensity was decreased slightly.

In transient absorption spectra during the ps laser excitation, even when the fluence is larger than that of the fs laser, the negative peak at 680 nm did not become a main component, in comparison to as in the fs laser excitation. It means that the dimer/aggregate is mainly excited, not the monomer. As the peak power of the ps laser is 1500 times lower than that of the fs laser, the simultaneous multiphoton absorption of the ground state monomer is inefficient, leading to inappreciable monomer depletion.

At a fluence of 112 mJ/cm², as the transient absorption spectra after relaxation of the excited states is similar to the temperature difference spectra of the ground state absorption shown in Fig. 5B, the transient absorption spectrum with negative bands at 600 and 680 nm and positive band at 710 nm is concluded to be hot band. Thus, the spectral change at the fluence of 112 mJ/cm² in a sub-ns time scale is attributed to a heating process through relaxation of the excited states. On the other hand, at the fluence of 9.7 mJ/cm², no drastic decay of the excited

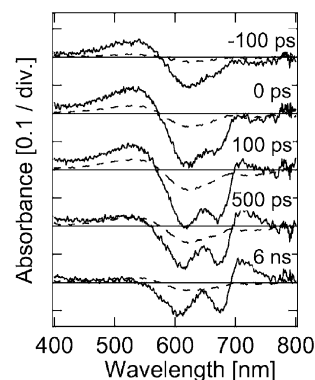


Fig. 8. Picosecond pump-fs probe absorption spectra at the laser fluence of 112 mJ/cm² (solid line) and 9.7 mJ/cm² (broken line). Delay times are given in the figure.

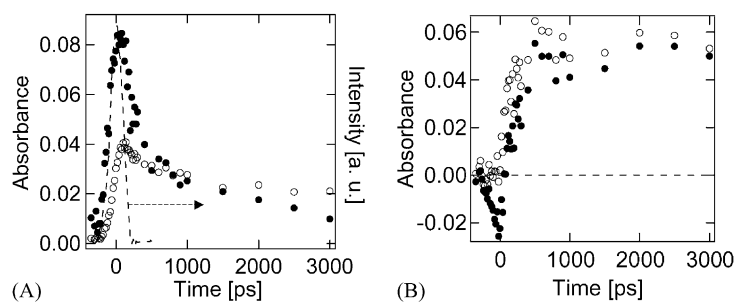


Fig. 9. (A) Temporal profiles of transient absorption at 520 nm at the laser fluence of 112 mJ/cm² (●) and 9.7 mJ/cm² (○) in ps pump-fs probe experiment. Dashed line in the figure represents a profile of the ps excitation pulse. (B) Corresponding time profiles of transient absorption at 710 nm (●) and estimated time evolution of hot band, Abs^{Hot}(710 nm, *t*) (○) (see text). The laser fluence is 112 mJ/cm².

states and no absorption meaning temperature elevation was observed.

The temporal profile of the absorption at 520 nm is shown in Fig. 9A. At the fluence of 112 mJ/cm², a rapid relaxation was observed within 200 ps, which is in the same order to the excitation pulse width. On the other hand, such a relaxation was not observed at 9.7 mJ/cm², so that the rapid decay is brought about only at high laser fluence. It is considered that the exciton–exciton annihilation produces an electronically higher excited states and a ground state. The higher excited states give off thermal energy rapidly upon the internal conversion to the lowest excited state, which gives a large amount of heat if the annihilation occurs densely.

The time profile at 710 nm at the fluence of 112 mJ/cm² is shown in Fig. 9B as a representative of the hot band. The negative absorption observed before 0 ps is assigned to bleaching of the ground state. Thus, the time profile in the time region from –150 to 50 ps is considered to be bleaching and recovery of the ground state. Here, we tried to extract the contribution of the hot band from the time profile by Eq. (2) under the following assumptions. (1) Only the excited states and the hot ground state are responsible to the present data and another species can be negligible. (2) The transient absorption spectral shape of the excited states is independent of the density. (3) The contribution of the hot band can be negligible at 520 nm. (4) The transient absorption spectrum

at –100 ps is due purely to the excited states.

$$\begin{aligned} \text{Abs}^{\text{Hot}}(710 \text{ nm}, t) \\ = \text{Abs}^{\text{Obs}}(710 \text{ nm}, t) - \text{Abs}^{\text{Obs}}(520 \text{ nm}, t) \\ \times \frac{\text{Abs}^{\text{Obs}}(710 \text{ nm}, -100 \text{ ps})}{\text{Abs}^{\text{Obs}}(520 \text{ nm}, -100 \text{ ps})}, \end{aligned} \quad (2)$$

where Abs^{Obs}(λ, *t*) is observed transient absorbance at the delay time, *t*, and Abs^{Hot}(λ, *t*) is the estimated absorbance of the hot band. The calculated result is shown as a function of the decay time in Fig. 9B. Abs^{Hot}(710 nm, *t*) corresponding to heat generation rises up to 200 ps and is constant over 6 ns which is the latest decay time in the present work. It means that the heat generation takes place up to 200 ps, and the attained temperature is kept at least for the ns time range. This is reasonable as the present excitation pulse has 250 ps fwhm. In the case of fs excitation, we have separately proposed that exciton–exciton annihilation and rapid photothermal conversion lead to heating in about 20 ps as described above. At almost the same laser fluence, the photothermal conversion in ps laser ablation is 10 times slower than that in fs laser ablation.

Fig. 10A shows fluence dependence of time profiles at 520 nm which are proportional to excited state density. In the time range up to 200 ps, the temporal profile was nearly common for the fluence of 60, 112, and 190 mJ/cm², although the decay after 200 ps is slightly depend on the

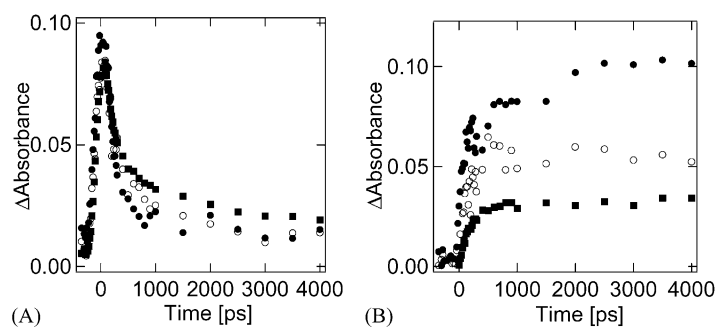


Fig. 10. (A) Temporal profiles of transient absorption at 520 nm at the laser fluence of 190 mJ/cm² (●), 112 mJ/cm² (○), and 60 mJ/cm² (■) in ps pump-fs probe experiment; (B) estimated time evolution of hot band, Abs^{Hot}(710 nm, *t*) (see text).

fluence. $\text{Abs}^{\text{Hot}}(710 \text{ nm}, t)$, corresponding to the amount of generated heat, is also given in Fig. 10B. We notice that an irregular increase of $\text{Abs}^{\text{Hot}}(710 \text{ nm}, t)$ was observed after 2 ns at the fluence of 190 mJ/cm^2 . As the fluence is about 2.5 times larger than the ablation threshold (80 mJ/cm^2), some surface morphological changes should be caused on this time scale, modifying optical measurements. The rise is observed in the time scale within 200 ps, which is the same time scale as relaxation of transient absorption at 520 nm.

The maximum of excited states density at 190 mJ/cm^2 is calculated to be 1.1 times larger than that at 60 mJ/cm^2 , although the former laser fluence is 3.2 times larger than the latter one. On the other hand, $\text{Abs}^{\text{Hot}}(710 \text{ nm}, t)$ at 190 mJ/cm^2 is 2.5 times larger than that at 60 mJ/cm^2 . It means that the total amount of generated heat increases with increasing fluence, although the excited states density is nearly same. This suggests that the absorption during excitation pulse is not proportional to the number of excited states formed and saturated with respect to laser fluence. Exciton–exciton annihilation takes place efficiently during the pulse, gives some heat, and reforms the ground state. The ground state then again absorbs excitation photons and again induces the annihilation. In the process, temporal excited state density will be saturated, because the annihilation is accelerated with increasing the fluence. On the other hand, as the process is repeatedly brought about during the pulse, the ejected thermal energy is accumulated giving heat, which is, namely, proportional to time-integrated density of the excited states relaxing to the ground state. Therefore, the amount of heat, corresponding to $\text{Abs}^{\text{Hot}}(710 \text{ nm}, t)$, will increase with the fluence because of acceleration of the annihilation. We conclude this cyclic multiphotonic absorption of the dimer/aggregate accelerated by exciton–exciton annihilation is responsible to the ps laser ablation. Nevertheless, increase of $\text{Abs}^{\text{Hot}}(710 \text{ nm}, t)$ is slightly smaller than the increase of the fluence, which suggests that some saturation of excited dimer/aggregate turns up under high laser fluence.

3.5. Photoabsorption, temperature elevation, and laser ablation mechanism

We have demonstrated that etching behaviours of SB film depend strongly on the excitation pulse duration (170 fs, 250 ps, 100 ns) at 780 nm. Above fs and ps ablation thresholds, the etch depth becomes constant and is almost independent of laser fluence, while the depth etched by ns laser excitation increases gradually with the fluence above its ablation threshold. The characteristic difference between fs/ps discrete and ns gradual etching behaviour can be examined by considering the effective thickness of excitation, temperature elevation and its dynamics, and surface morphology changes which are initial primary processes of laser ablation. As the film thickness is thinner (600 nm) than the penetration depth of the 780 nm excitation pulse

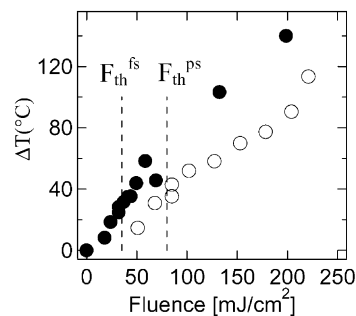


Fig. 11. Temperature elevation (ΔT) vs. laser fluence upon irradiation with fs (●) and ps (○) excitation pulses estimated by using Eq. (1) (see text). $F_{\text{th}}^{\text{fs}}$ and $F_{\text{th}}^{\text{ps}}$ in figure are thresholds of fs and ps laser ablation, respectively.

($1/\alpha = 1.4 \mu\text{m}$ for the dimer/aggregate molecule), it is considered that the excitation pulse produces excited states homogeneously along the depth even for ns excitation. Furthermore, fs and ps excitation causes various saturation leading to deeper excitation. These mean photothermal conversion takes place uniformly and its time scale was measured to be 20 and 200 ps for fs and for ps excitation, respectively. Temperature elevation is estimated by comparing transient absorption at 1 ns and temperature difference spectra and by using Eq. (1), and plotted as a function of laser fluence, which is displayed in Fig. 11. The conversion efficiency is higher in fs excitation than in ps, which may be ascribed to their different photoabsorption processes. In case of fs excitation, the CuPc dimer/aggregate is depleted and the monomer is also excited, indicating efficiently multiphoton absorption as described above. Picosecond excitation is induced in terms of cyclic multiphotonic photoabsorption by the dimer/aggregate accelerated by exciton–exciton annihilation. It is worth noting that fs and ps absorption is induced when temperature elevation of 30°C is attained.

Interestingly, the temperature attained is not so high as to cause sublimation and chemical decomposition of CuPc molecules. The sublimation starts at 380°C and decomposition reaction is induced over 550°C [49]. Thus, absolute thermal energy does not explain the low threshold. Here, we introduce our recent results on time-resolved light scattering imaging of laser-induced surface morphological dynamics of the present amorphous CuPc film. Initial surface morphological changes of laser ablation were observed as generation of nm surface roughness only after a few ns [34]. Thus, the relations between photoexcitation, temperature elevation, and morphological change are summarised for fs, ps, and ns excitation in Fig. 12. It is worth noting there are some time lags between the heating and morphological changes, which we considered the key to understand the excitation pulse duration dependent etching; discrete and gradual. The area surrounding of the homogeneously excited area of the film is cold, and at the bottom is a quartz substrate. Vigorous molecular motions increasing due to heating accumulate in the film, which should generate transient pressure [50,51].

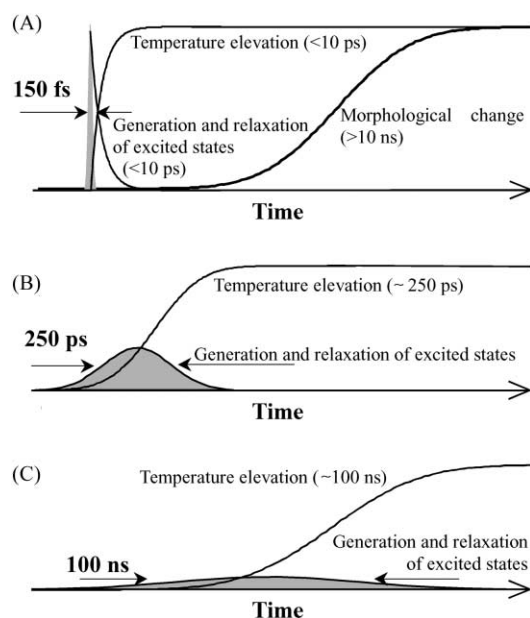


Fig. 12. The time evolution of photothermal processes and morphological change when (A) fs, (B) ps, and (C) ns pulses were applied as the excitation pulse.

When the pressure increased during the lag time reaches certain threshold, it should be released by splitting the film into two. Consequently, the interface layer facing the substrate remains and the other surface layer is ejected; thus, discrete etching is thus brought about.

On other hand, in the ns ablation, it is considered that photothermal conversion process and morphological change progress on the same time scale, as schematically shown in Fig. 12C. This was confirmed by ns transient absorption spectroscopy and ns interferometry already reported [52,53]. The photothermal conversion process will be again due to the cyclic multiphotonic absorption and the excited states will not saturate. In the ns case, however, the ground state can be sufficiently recovered by itself as the lifetime of CuPc excited states is much shorter than the 100 ns pulse duration [52]. Since vigorous molecular motions can increase gradually with heating in the 100 ns time range, no appreciable transient pressure will be induced. However, the surface can still be heated and an explosive sublimation should be induced. As the etch depth will increase with increasing amount of generated heat, it will increase gradually with the fluence. It is reasonable that the ablation threshold is higher than in the fs and ps cases.

4. Conclusion

The excitation energy relaxation processes of SB film and the excitation pulse duration effects have been investigated and confirmed by fs pump-fs probe and ps pump-fs probe UV–VIS absorption spectroscopy. Regardless of the

excitation pulse width, electronically excited states and hot ground states are observed as transient species and responsible for effective photothermal conversion. The hot band population clearly increased with the relaxation of the excited states, whose dynamics depends on the pulse duration. In case of fs excitation, the CuPc dimer/aggregate in SB film is depleted and the monomer is additionally excited, indicating efficient multiphoton absorption. In ps excitation, cyclic multiphotonic absorption of excitations photons by the dimer/aggregate is accelerated by exciton–exciton annihilation. The time scale of the photothermal conversion induced by fs, ps, and ns pulse was confirmed to be 20 ps, 200 ps, and 100 ns, respectively. On the base of our recent result that nm surface roughness in the ablation is formed in a few ns time scale [34], it is proposed that there is a time lag between photothermal conversion and morphological change. Thus, a transient high pressure should be brought about for the fs and ps ablation and the pressure will cause mechanical disruption leading to the discrete etching. On the other hand, in the ns ablation, no appreciable transient pressure is induced and heating of surface in the 100 ns time range causes an explosive sublimation giving gradual etching.

Acknowledgements

This work is partly supported by Special Coordination Funds for Promoting Science and Technology on “Development of high-density optical pulse generation and advanced material control technology” to TA and by the Grant-in-Aid on Priority Area (B) for “Laser chemistry of single nanometre organic particles” (10207204) to HM from the Ministry of Education, Science, Sports, and Culture, Japan.

References

- [1] R.G.W. Norrish, G. Porter, *Nature* 164 (1949) 658.
- [2] G.R. Fleming, *Chemical Application of Ultrafast Spectroscopy*, Oxford University Press, New York, 1986.
- [3] J. Manz, L. Wouste (Eds.), *Femtosecond Chemistry*, Wiley-VCH, Weinheim, 1995.
- [4] D.H. Auston, C.V. Shank, *Phys. Rev. Lett.* 32 (1974) 1120.
- [5] E. Tokunaga, A. Terasaki, T. Kobayashi, *Phys. Rev. A* 47 (1993) 4581.
- [6] E. Tokunaga, A. Terasaki, T. Kobayashi, *J. Opt. Soc. Am. B* 12 (1995) 753.
- [7] D.G. Avery, *Proc. Phys. Soc. B* 65 (1952) 425.
- [8] I. Simon, *J. Opt. Soc. Am.* 41 (1951) 336.
- [9] M.R. Querry, *J. Opt. Soc. Am.* 59 (1969) 876.
- [10] R.M.A. Azzam, *J. Opt. Soc. Am.* 72 (1982) 1439.
- [11] M. Ichikawa, H. Fukumura, H. Masuhara, *J. Phys. Chem.* 98 (1994) 12211.
- [12] M. Ichikawa, H. Fukumura, H. Masuhara, A. Koide, H. Hyakutake, *Chem. Phys. Lett.* 232 (1995) 346.
- [13] M. Ichikawa, H. Fukumura, H. Masuhara, *J. Phys. Chem.* 99 (1995) 12072.
- [14] Y. Hosokawa, K. Watanabe, T. Asahi, H. Fukumura, H. Masuhara, *Bull. Chem. Soc. Jpn.* 72 (1999) 909.

- [15] R.W. Kessler, F. Wilkinson, *J. Chem. Soc., Faraday. Trans. I* 77 (1981) 309.
- [16] R.W. Kessler, G. Krabichler, S. Uhl, D. Oelkrug, W.P. Hagan, J. Hyslop, F. Wilkinson, *Opt. Acta* 30 (1983) 1099.
- [17] P. Kubelka, F. Munk, *Z. Tech. Phys.* 12 (1931) 593.
- [18] N. Ikeda, K. Imagi, H. Masuhara, N. Nakashima, K. Yoshihara, *Chem. Phys. Lett.* 140 (1987) 281.
- [19] N. Ikeda, M. Koshioka, H. Masuhara, K. Yoshihara, *Chem. Phys. Lett.* 150 (1988) 452.
- [20] N. Fukazawa, H. Fukumura, H. Masuhara, J. Prochorow, *Chem. Phys. Lett.* 220 (1994) 461.
- [21] T. Asahi, A. Furube, H. Fukumura, M. Ichikawa, H. Masuhara, *Rev. Sci. Instrum.* 69 (1998) 361.
- [22] A. Furube, T. Asahi, H. Masuhara, *Jpn. J. Appl. Phys.* 38 (1999) 4236.
- [23] A. Furube, T. Asahi, H. Masuhara, H. Yamashita, M. Anpo, *Chem. Lett.* (1997) 735.
- [24] A. Furube, T. Asahi, H. Masuhara, H. Yamashita, M. Anpo, *J. Phys. Chem. B* 103 (1999) 3120.
- [25] A. Furube, T. Asahi, H. Masuhara, H. Yamashita, M. Anpo, *Res. Chem. Intermed.* 27 (2001) 177.
- [26] H. Fukumura, E. Takahashi, H. Masuhara, *J. Phys. Chem.* 99 (1995) 750.
- [27] R. Srinivasan, B. Braren, K.G. Casey, *J. Appl. Phys.* 68 (1990) 1842.
- [28] H. Furutani, H. Fukumura, H. Masuhara, *J. Phys. Chem.* 100 (1996) 6871.
- [29] H. Furutani, H. Fukumura, H. Masuhara, T. Lippert, A. Yabe, *J. Phys. Chem. A* 101 (1997) 5742.
- [30] H. Furutani, H. Fukumura, H. Masuhara, S. Kambara, T. Kitaguchi, H. Tsukada, T. Ozawa, *J. Phys. Chem. B* 102 (1998) 3395.
- [31] T. Mito, T. Masubuchi, T. Tada, H. Fukumura, H. Masuhara, *J. Photosci.* 6 (1999) 109.
- [32] T. Masubuchi, H. Furutani, H. Fukumura, H. Masuhara, *Chem. Phys. Chem.* 3 (2000) 137.
- [33] K. Hatanaka, T. Itoh, T. Asahi, N. Ichinose, S. Kawanishi, T. Sasuga, H. Fukumura, H. Masuhara, *Appl. Phys. Lett.* 73 (1998) 3498.
- [34] Y. Hosokawa, M. Yashiro, T. Asahi, H. Fukumura, H. Masuhara, *Appl. Surf. Sci.* 154 (2000) 192.
- [35] Y. Hosokawa, M. Yashiro, T. Asahi, H. Masuhara, *Proc. SPIE* 4274 (2001), 78.
- [36] H. Fukumura, H. Masuhara, *Chem. Phys. Lett.* 221 (1994) 373.
- [37] K. Watanabe, T. Asahi, H. Fukumura, H. Masuhara, K. Hamano, T. Kurata, *J. Phys. Chem. B* 101 (1997) 1510.
- [38] Y. Hosokawa, K. Watanabe, T. Asahi, H. Fukumura, H. Masuhara, Y. Imanishi, *Mol. Cryst. Liq. Cryst.* 314 (1998) 59.
- [39] R. Srinivasan, E. Sutcliffe, B. Braren, *Appl. Phys. Lett.* 51 (1987) 1285.
- [40] S. Küper, M. Stuke, *Appl. Phys. B* 44 (1987) 199.
- [41] S. Preuss, M. Späth, Y. Zhang, M. Stuke, *Appl. Phys. Lett.* 62 (1993) 3049.
- [42] G.H. Pettit, R. Sauerbrey, *Appl. Phys. A* 56 (1993) 51.
- [43] H. Kumagai, K. Midorikawa, K. Toyoda, S. Nakamura, T. Okamoto, M. Obara, *Appl. Phys. Lett.* 65 (1994) 1850.
- [44] Z. Bor, B. Racz, G. Szabo, D. Xenakis, C. Kalpouzos, C. Fotakis, *Appl. Phys. A* 60 (1995) 365.
- [45] E.A. Lucia, F.D. Verderame, *J. Chem. Phys.* 48 (1968) 2674.
- [46] M. Ichikawa, Ph.D. Thesis, Osaka University, Osaka, 1994.
- [47] V. Gulbinas, M. Chachisvilis, L. Valkunas, V. Sundström, *J. Phys. Chem.* 100 (1996) 2213.
- [48] A. Terasaki, M. Hosoda, T. Wada, H. Tada, A. Koma, A. Yamada, H. Sasabe, A.F. Garito, T. Kobayashi, *J. Phys. Chem.* 96 (1992) 10534.
- [49] E.A. Lawton, *J. Phys. Chem.* 62 (1958) 384.
- [50] D.D. Dlott, S. Hambr, J. Franken, *J. Phys. Chem. B* 102 (1998) 2121.
- [51] L.V. Zhigilei, B. Garrison, *Appl. Surf. Sci.* 127 (1998) 142.
- [52] H. Fukumura, Y. Yoneda, H. Takahashi, H. Masuhara, *Chem. Lett.* (1996) 509.
- [53] M. Hosoda, H. Furutani, H. Fukumura, H. Masuhara, M. Nishii, N. Ichinose, S. Kawanishi, *Rev. Laser Eng.* 25 (1997) 306.